Self-similar flow and contact line geometry at the rear of cornered drops

Jacco H. Snoeijer, Emmanuelle Rio, Nolwenn Le Grand, and Laurent Limat
Laboratoire de Physique et Mécanique des Milieux Hétérogènes and Fédération de Recherche Matière et Systèmes Complexes [Unite Mixte de Recherche (UMR) Centre National de la Recherche Scientifique (CNRS) 7636 and Fýdýration de Recherche (FR) Centre National de la Recherche Scientifique (CNRS) 2438], ESPCI, 10 rue Vauquelin 75005, Paris, France

Partially wetting drops sliding down an inclined plane develop a "corner singularity" at the rear, consisting of two dynamic contact lines that intersect. We analyze the three-dimensional flow in the vicinity of this singularity by exploring similarity solutions of the lubrication equations. These predict a self-similar structure of the velocity field, in which the fluid velocity does not depend on the distance to the corner tip; this is verified experimentally by particle image velocimetry. The paper then addresses the small-scale structure of the corner, at which the singularity is regularized by a nonzero radius of curvature R of the contact line. Deriving the lubrication equation up to the lowest order in $1/R$, we show that contact line curvature postpones the destabilization of receding contact lines to liquid deposition, and that $1/R$ increases dramatically close to the "pearling" instability. The general scenario is thus that sliding drops avoid a forced wetting transition by forming a corner of two inclined contact lines, which is regularized by a rounded section of rapidly decreasing size. © *2005 American Institute of Physics*. [DOI: 10.1063/1.1946607]

I. INTRODUCTION

Wetting and dewetting phenomena are encountered in many everyday life situations, such as drops sliding down a window or meandering rivulets. However, the description of moving contact lines, separating wet from dry regions, remains controversial; in classical hydrodynamics the viscous stresses diverge at the contact line.[1,2] This viscous flow near the contact line is driven by capillary forces and gives rise to extremely curved interfaces, even down to the microscopic molecular scale. To release the hydrodynamic singularity one has to include the microscopic physics near the contact line, for which various approaches have been proposed.[3–12] Wetting dynamics thus involves length scales ranging from a microscopic length up to the capillary length, and forms a challenge that is not only of fundamental interest; dynamic contact lines are crucial in many industrial applications such as coating and painting.[13]

A particularly intriguing phenomenon is that *receding* contact lines become unstable beyond a critical speed.[14–22] This "forced wetting transition" can be studied by withdrawing a solid plate with a velocity U_0 from a bath of partially wetting liquid; a liquid film is deposited above a critical value of the capillary number Ca$= \eta U_0/\gamma$, where η and γ denote the viscosity and surface tension of the liquid. This instability exemplifies that the physics at the contact line has macroscopic consequences, since the critical Ca strongly depends on the contact angle at the microscopic scale.[15,16] Even though close to the contact line the system is far from equilibrium, one usually makes the strong assumption of imposing the equilibrium contact angle. Another open question is what happens beyond the critical velocity. In particular, the contact line geometry often becomes truly three dimensional; Blake and Ruschak[20] observed contact lines inclined with respect to the horizontal—this reduces the normal velocity of the contact line such that the wetting transition is avoided. A similar structure appears at the rear of sliding drops,[23,24] which develops a sharp corner [Fig. 1(a)]. In all these experiments, the normal velocity of the inclined contact lines was found to stay precisely at the threshold of instability, which implies that the half opening angle, Φ, scales as $\sin \Phi \propto 1/$Ca [Fig. 2(c)]. Note that in some cases receding contact lines can develop a transverse instability, with a finite wavelength along the contact line, as observed, e.g., for liquid ridges on an inclined plane[25,26] or dewetting of polymeric liquids.[27]

In this paper we unravel the singular three-dimensional flow that occurs in "cornered" sliding drops, both theoretically and experimentally. The first part of the paper forms a full exposition and expansion of the self-similar hydrodynamic model of a sharp cone [Fig. 1(c)], which has been proposed in previous papers.[28,29] In this approach the liquid thickness is described by a similarity function of space variables, which is a common strategy near surface singularities. Indeed, the corner is reminiscent of other hydrodynamic singularities, such as the pinching of a jet into droplets,[30] the selective withdrawal transition,[31] or the formation of a cusp between two rotating immersed cylinders.[32] For the first time, however, we investigate the self-similar velocity fields and provide a detailed comparison with experimental measurements using particle image velocimetry. Figures 1(b) and 1(d) show the experimental and theoretical flow fields, respectively, which display a very good agreement. Our measurements reveal that the structure of the velocity field does not depend on the distance to the corner tip, and confirm the predictions of the similarity solutions also quantitatively. Particular attention will be paid to the flow near the contact line, which turns out to be oriented perpendicularly to the contact line.[33]

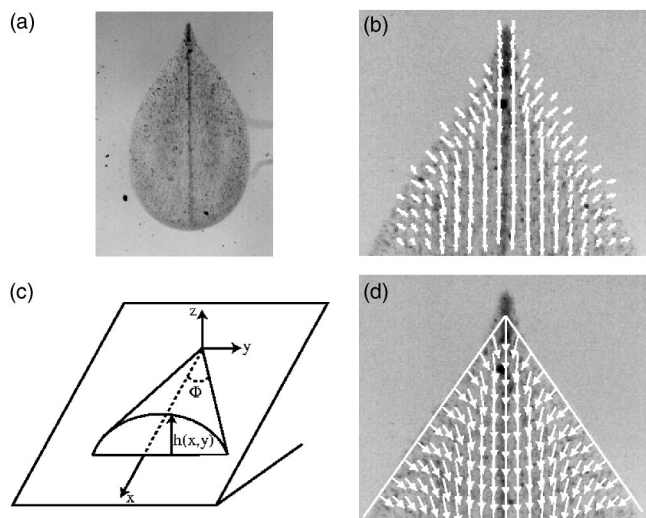**17**, 072101-1

(a)

(b)

(c)

(d)

FIG. 1. (a) A silicon oil drop sliding down a glass plate coated with fluoropolymers develops a singularity at the rear above a critical velocity. (b) The corresponding velocity field in the laboratory frame visualized by tracer particles using particle image velocimetry. (c) and (d) Modeling the interface by a sharp cone, we quantitatively reproduce the experimental velocity field, except at the very tip of the singularity; this cusp-like structure does not seem to affect the velocity field away from the tip.

In the second part of the paper we investigate the transition from rounded drops to cornered drops in more detail. As can be seen from the photographs in Fig. 2, the corner at the rear of the drop is never infinitely sharp but has a nonzero radius of curvature R; there is a small-scale cutoff at which the singularity is regularized. This is in conflict with the assumption of a sharp cone[29] as well as with the prediction of another recent model based upon a gravity-capillary balance.[34] Despite this rounded edge there is still a well-defined corner angle Φ, following from the two nearly
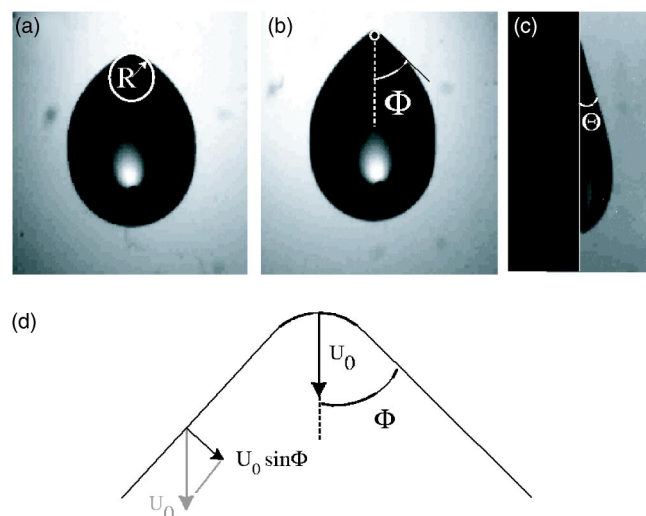
(a)

(b)

(c)

(d)

FIG. 2. (a) and (b) Increasing the sliding velocity U_0, one encounters a transition from rounded to cornered drops that is characterized by a rapid decrease of the radius of curvature, R, of the rear. (c) Side view of the drop shown in (b), from which the apparent macroscopic contact angle θ is extracted. (d) The corner angle Φ is defined from the (nearly) straight inclined contact lines at the side of the drop; their normal velocity, $U_0 \sin \Phi$, is observed to remain constant Refs. 20, 23, and 24.

straight inclined contact lines away from the rear. Recent measurements show that R rapidly decreases as a function of drop velocity when Φ becomes smaller than 90°.[35]

Such a finite radius of curvature, however, puts forward an intriguing paradox; while the normal velocity of the inclined contact lines $U_0 \sin \Phi$ is maintained at the maximum speed of dewetting, the velocity at the rear remains U_0 and thus exceeds this critical speed [Fig. 2(d)]. In other words, a straight contact line moving at such a high velocity would be forced to emit little droplets or to leave a film. To resolve this problem we develop a one-dimensional description for *curved contact lines*, which takes this curvature into account up to the lowest order. We show that this gives rise to additional capillary forces that are responsible for an increase of the maximum speed of dewetting with $1/R$. This lowest-order model provides a satisfactory agreement with experimental results.

The paper is organized as follows. In Sec. II we consider the lubrication equations in the limit of Stokes flow, from which we derive the general formalism leading to the similarity solutions. In Sec. III we discuss the predictions of the model concerning both the structure of the velocity field and that of the free surface. We then compare the obtained velocity fields to particle image velocimetry (PIV) measurements performed on silicon oil drops sliding on a glass plate coated with fluoropolymers in Sec. IV. In Sec. V we investigate the curved "core" of the singularity by developing a model of dynamic curved contact lines. We derive the lubrication equation in the limit of small contact line curvature and show that the additional curvature postpones the forced wetting transition. The paper closes with a discussion in Sec. VI.

II. HYDRODYNAMIC DESCRIPTION OF FLOW IN A CORNER GEOMETRY

A. Physics of three-dimensional corner flow

We will first investigate some general aspects of the three-dimensional flow occuring at the rear of a sliding drop exhibiting a corner. Indicating the location of the interface by $z = h(x,y)$, we consider drops of conical shape

$$h(x,y) \propto xH(y/x), \tag{1}$$

where the definitions of the axes are given in Fig. 1(c). We thus assume that cross sections at a given distance x are self-similar and depend only on the ratio y/x. Since in the experiments of Refs. 23 and 24 the drops flow at low-Reynolds numbers, the flow can be described by the Stokes equations,

$$\nabla \cdot \mathbf{u} = 0, \tag{2}$$

$$-\nabla p + \eta \Delta \mathbf{u} = \mathbf{0}, \tag{3}$$

where the three-dimensional velocity field $\mathbf{u}$ and the pressure p are functions of the spatial coordinates x, y, and z. The height at the rear of the drop will be well below the capillary length $l_\gamma = \sqrt{\gamma/\rho g}$, so we have omitted the gravitational forces in Eq. (3). In this regime the viscous flow is entirely driven by the capillary pressure at the free surface $p = \gamma \kappa$, where κ is the mean curvature of the interface. It is clear that

the capillary number $\mathrm{Ca}=\eta U_0/\gamma$ becomes the relevant dimensionless parameter describing the balance between viscous and capillary forces.

One can now recover the scaling behavior of the corner flow from a simple dimensional analysis. For the interface height described by Eq. (1), the only length scale is provided by x, the distance to the corner. The curvature κ, and hence the pressure, therefore have to scale as $1/x$. Following Eq. (3) we obtain $\Delta\mathbf{u}=\mathcal{O}(1/x^2)$, so that the velocity field itself should only depend on the combinations y/x and z/x; since all lengths are now rescaled by x, this yields a Laplacian $\sim 1/x^2$. One can indeed show that Eqs. (2) and (3) allow scaling solutions of the type

$$\mathbf{u}(x,y,z) = \tilde{u}\left(\frac{y}{x},\frac{z}{x}\right),$$

$$p(x,y,z) = \frac{1}{x}\tilde{p}\left(\frac{y}{x},\frac{z}{x}\right). \tag{4}$$

The relevance of these corner solutions will be illustrated in Sec. IV, where we present experimental measurements of the velocity fields. Indeed, we observe a large range of distances from the corner tip in which the velocity only depends on y/x, supporting the hypothesis of a self-similar corner profile. To make a more quantitative comparison for both the velocity fields as well as geometrical properties of the cone, we will explicitly resolve the flow equations within the lubrication limit for which $h/x\ll 1$.

B. Corner flows: Three-dimensional capillary forces

Before we continue the analysis, let us briefly discuss the driving mechanisms of the flow in the corner. In order to maintain a viscous flow one requires gradients of (capillary) pressure; the height of the drop at the rear is too small for gravity to play a role. Let us first consider the flow at the central axis of the drop, which is located at $y=0$. Due to symmetry, the local fluid velocity will be purely along the downward x direction. At this symmetry axis the interface of the cone is flat along x, but curved along the y direction. Since cross sections at fixed distance from the rear x do not change shape but are simply scaled by x, this "transverse" radius of curvature increases with x; this results in a decreasing capillary pressure, and hence provides a driving force. So at the symmetry axis of the drop, the flow is entirely driven by gradients of the *transverse curvature*.

This is very different from the flow near a one-dimensional moving (straight) contact line, which is the common theoretical benchmark for contact line dynamics. In this case the flow is perpendicular to the contact line. In the direction perpendicular to the flow, the interface is flat, so there is no transverse curvature; the driving force is now provided by strong curvatures of the interface *along* the flow direction. While globally the flow in the corner geometry is more complicated, we will show that the physics near the contact line at $y/x=\tan\Phi$ reduces to that of a one-dimensional (1D) moving contact line.

C. Lubrication approximation

We will now briefly repeat the derivation of the equation for $H(y/x)$ in the well-known lubrication approximation, as presented by Limat and Stone.[29] In the limit of small angles it is well known that the velocity field becomes parallel to the inclined plane ($u_z\approx 0$) and has a simple Poiseuille-like parabolic vertical dependence. With the no-slip boundary condition at the bottom plate the viscous term in Eq. (3) becomes $-3\eta\mathbf{U}/h^2$, where

$$\mathbf{U}(x,y) = \frac{1}{h}\int_0^h dz\,\mathbf{u}(x,y,z). \tag{5}$$

Another consequence of $u_z\approx 0$ is that the pressure becomes independent of z and simply reads $p(x,y)=-\gamma\Delta h$, so that Eq. (3) reduces to

$$\boldsymbol{\nabla}\Delta h - \frac{3\eta}{\gamma}\frac{\mathbf{U}}{h^2} = \mathbf{0}, \tag{6}$$

where $\mathbf{U}$ is the two-dimensional (2D) depth-averaged velocity in the frame attached to the inclined plane. Throughout the paper we always work in this laboratory frame. Note that $\mathbf{U}$ represents a local fluid velocity, which, in general, will be different from the global drop velocity. This equation should be complemented with the depth-averaged mass continuity equation

$$\partial_t h + \boldsymbol{\nabla}\cdot(h\mathbf{U}) = 0. \tag{7}$$

Drops sliding at constant velocity U_0 with constant shape can be described by an interface $h(x-U_0 t,y)$, so that upon elimination of $\mathbf{U}$, we obtain an equation for $h(x,y)$,

$$3\mathrm{Ca}\,\partial_x h = \boldsymbol{\nabla}\cdot[h^3\boldsymbol{\nabla}\Delta h], \tag{8}$$

where $\mathrm{Ca}=\eta U_0/\gamma$ is the capillary number. If we now insert the similarity ansatz

$$h(x,y) = \mathrm{Ca}^{1/3}xH(\zeta), \quad \text{with } \zeta=\frac{y}{x}, \tag{9}$$

one obtains an equation for $H(\zeta)$,

$$(1+\zeta^2)^2(H^3 H_{\zeta\zeta\zeta})_\zeta + 3\zeta(1+\zeta^2)(H^3 H_{\zeta\zeta})_\zeta + 2\zeta(1$$
$$+ \zeta^2)H^3 H_{\zeta\zeta\zeta} + (1+3\zeta^2)H^3 H_{\zeta\zeta} = 3(H-\zeta H_\zeta). \tag{10}$$

This equation no longer depends explicitly on the capillary number Ca.

D. Boundary conditions

The corner profile $H(\zeta)$ is governed by a fourth-order equation, so we have to specify four boundary conditions. Due to symmetry around $\zeta=0$ we have to impose $H'(0)=H'''(0)=0$, so one is left with two free parameters $H(0)$ and $H''(0)$. As an example, Fig. 3(a) displays numerical solutions of Eq. (10) that have $H(0)=3$, but with different initial curvatures $H''(0)$; a similar scenario is found for other $H(0)$. One sees that for small initial curvatures the solutions do not tend to zero, but, in fact, have a minimum height. This clearly does not correspond to the situation of a droplet with
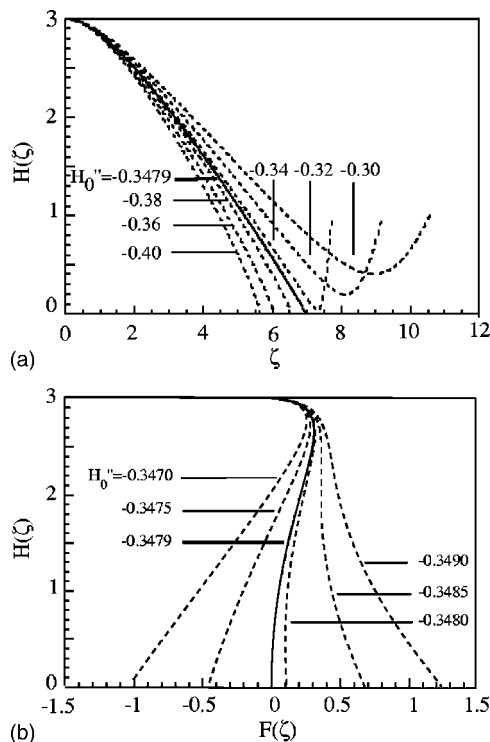
FIG. 3. (a) Solutions of Eq. (10) with $H(0)=3$ for different initial curvatures $H''(0)$. The solid line represents the separatrix between solutions that have a minimum and solutions that tend to zero. (b) Only this separatrix obeys global mass conservation; the total integrated flux $F(\zeta)$ should vanish as $H(\zeta)$ becomes zero (Ref. 36).

a contact line; in fact, we show below that there is a nonzero flux of liquid from the "droplet" into the "reservoir" region to the right of the minimum.

For strongly negative $H''(0)$, on the other hand, the solutions do tend to zero and one encounters the usual contact line singularity as $H \to 0$. In general, however, these solutions violate global conservation of mass; in order to be a physically reasonable solution of a drop sliding at steady state, it is necessary that in the frame comoving with the drop, the x flux integrated over a cross section is zero.[29] This argument is expressed mathematically by calculating the x flux between $y=-\zeta x$ and $y=\zeta x$, which will be denoted by $F(\zeta)$,

$$ F(\zeta) = \int_0^\zeta d\zeta' H^3 \left([\zeta'(\zeta'^2 + 1)H_{\zeta'\zeta'}]_{\zeta'} + \frac{3}{H^2} \right). \quad (11) $$

For a derivation of this integral we refer to Ref. 29. This flux should vanish when $H(\zeta)$ tends to zero. In Fig. 3(b) we therefore show a parametric plot of $F(\zeta)$ vs $H(\zeta)$; only a single curve obeys the zero-flux condition when approaching the contact line. Hence for each $H(0)$ there is a unique $H''(0)$ that corresponds to a physical solution of the problem.

Let us now argue that this physical solution is precisely the *separatrix* between the solutions that tend to zero and the solutions that display a minimum in Fig. 3. We already mentioned above that whenever H has a minimum, the fluid velocity is directed from the drop region into the reservoir region. This can be understood directly from Fig. 3(a); the increase of H'' when approaching the minimum yields a de-

crease of capillary pressure along ζ. This results in a nonzero "outward" flux $hU_\perp$. When approaching the separatrix, however, the height of the minimum will ultimately tend to zero and hence yield a vanishing flux $hU_\perp \to 0$.

In the regime to the left of the separatrix, on the other hand, one truly encounters the singularity. Close to the contact line at $\zeta_c = \tan \Phi$, Eq. (10) will be dominated by the highest derivatives and reduces to $(1+\zeta_c^2)^2(H^3 H_{\zeta\zeta\zeta})_\zeta = -3\zeta_c H_\zeta$. This equation can be integrated once,

$$ (1 + \tan^2 \Phi)^2 H''' = -\frac{3 \tan \Phi}{H^2} + \frac{c}{H^3}, \quad (12) $$

where c is the integration constant. First, note that this equation has the same structure as the lubrication equation for a one-dimensional contact line, which reads $h''' = -3\mathrm{Ca}/h^2$. Second, we show in Sec. III that the fluid velocity close to the contact line is proportional to $H^2 H'''$, so that only the solution with $c=0$ corresponds to a finite velocity. For $c<0$, the singularity gives rise to an unphysical source term at the contact line, which yields a nonzero global flux. For $c>0$, on the other hand, the sign of the derivatives will change at $H=c/(3 \tan \Phi)$, which will later on give rise to a minimum. There is thus a single value of $H''(0)$ that corresponds to the physical solution, which verifies $c=0$.

To summarize, we have identified a one-parameter family of self-similar corner profiles. In order to make a comparison with experiments, it is convenient to simply parametrize the solutions by the corner angle $\Phi = \arctan \zeta_c$, where ζ_c indicates the location where $H \to 0$. This illustrates the strength of our analysis; for each value of the corner angle the model provides a prediction without any adjustable parameters.[29]

III. RESULTS FOR THE SELF-SIMILAR CORNER MODEL

A. Velocity profiles

Perhaps the most interesting feature of the corner model is that it predicts the nontrivial two-dimensional velocity field that occurs within the corner singularity. Using Eq. (6), this velocity field follows from the height profile as $\mathbf{U} = (\gamma/3\eta)h^2 \nabla \Delta h$. Numerical evaluations of this equation lead to the vector representation of flow fields displayed in Figs. 4(a) and 4(b), for two typical values of the opening angle Φ.

Upon a close inspection of these velocity fields one finds that, close to the contact line, the direction of fluid flow always becomes perpendicular to the contact line. To elucidate this intringuingly robust observation it is convenient to introduce cylindrical coordinates, $x=r \cos \varphi$, $y=r \sin \varphi$, and to consider the radial and azimuthal velocity components, U_r and U_φ, respectively. We use the symbol φ to indicate the angle within the corner, so that $-\Phi \le \varphi \le \Phi$. The velocity components U_r and U_φ are plotted next to the vector fields in Figs. 4(c) and 4(d). At the symmetry axis $\varphi=0$, the flow is always purely radial as expected, since $U_\varphi=0$. Note that at $\varphi=0$ the velocity U_r is always larger than U_0.[37] At the contact line ($\varphi=\Phi$), on the other hand, the radial component vanishes and the flow becomes purely perpendicular to the contact line. This property of perpendicular flow near a mov-
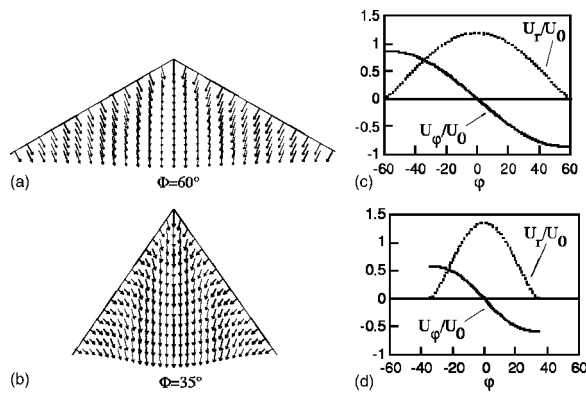
FIG. 4. On the left we show the velocity fields as predicted by the corner model for two opening angles, $\Phi=60°$ and $\Phi=35°$. The plots on the right represent the corresponding radial velocity U_r (dotted line) and the azimuthal velocity U_φ (solid line). Since $U_r=0$ at $\varphi=\Phi$, the velocity is locally perpendicular to the contact line.

FIG. 5. Relationship between the corner angle Φ and $H_0=\tan\theta/\mathrm{Ca}^{1/3}$. The solid line is obtained by numerical solution of Eq. (10), which for small angles takes the asymptotic form of Eq. (14) (dashed line). The symbols are experimental data on drops of silicon oil for various viscosities, from Ref. 35.

ing contact line is not special for the corner model, but, in fact, it constitutes a fundamental property of moving contact lines;[33] a tangential velocity component would require diverging (or at least extremely large) gradients of the curvatures of the contact line itself. Hence, for macroscopically straight contact lines, i.e., contact lines with radius of curvature much larger than the molecular scale, the tangential velocity component has to vanish. We have been able to experimentally confirm this property of perpendicular flow near the contact line, both in the corner regime (Sec. IV) and for rounded drops.[33]

In order to discuss the physics near the contact line in more detail, let us consider the explicit expressions of U_r and U_φ in terms of H,

$$\frac{U_r}{U_0} = -\frac{1}{3}H^2H''\cos\varphi(1+\tan^2\varphi),$$

$$\frac{U_\varphi}{U_0} = \frac{1}{3}H^2\cos\varphi(1+\tan^2\varphi)$$

$$\times[3H''\tan\varphi+H'''(1+\tan^2\varphi)]. \tag{13}$$

These velocity components are independent of the radial distance r. As we saw in Fig. 4, the radial velocity U_r vanishes at the contact line. According to Eq. (13) this implies that $H^2H''\to0$ as $H\to0$. At the same time U_φ, and hence H^2H''', remains finite. This is consistent with Eq. (12); the physical solution for which $c=0$ has $H^2H'''=-3\tan\Phi/(1+\tan^2\Phi)^2$. Inserting this into the expression for U_φ, one finds that $U_\varphi=-U_0\sin\Phi$. Hence, we find that at the contact line, the local fluid velocity coincides with the normal velocity of the moving contact line. In this respect, the hydrodynamics close to the contact line in the corner regime is really the same as that of a 1D contact line with a reduced velocity $U_0\sin\Phi$.

B. Geometrical properties

The corner model also provides a prediction for the geometrical properties of the interface. From Fig. 1(c) it can be seen that the cone has two characteristic angles that are easily measured experimentally; the angle in the (x,y) plane at
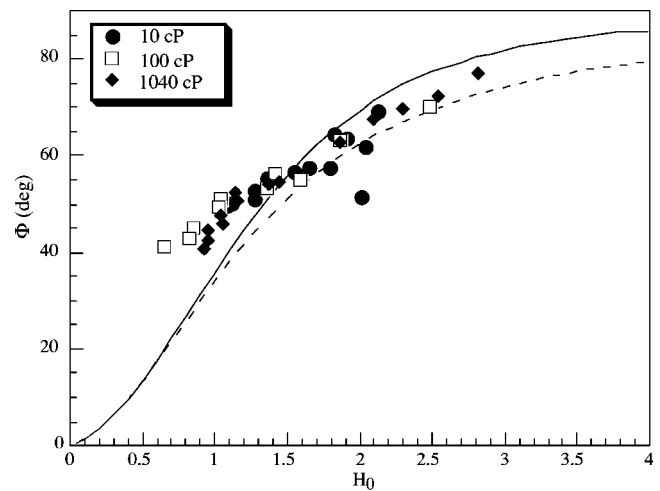
$z=0$, which is twice the corner angle Φ, and the angle in the (x,z) plane at $y=0$. The second angle can be measured from a side view of the drop as the apparent contact angle θ [Fig. 2(c)].

The value of $\tan\theta$ can be obtained directly from Eq. (9) as $\tan\theta=H(0)\mathrm{Ca}^{1/3}$. The model thus provides a relation between θ and Φ, since $H(0)$ is uniquely related to Φ. This is illustrated by the solid line in Fig. 5, showing Φ as a function of $H(0)$. The symbols appearing in the same figure have been deduced from experimental measurents of θ, via $H(0)=\tan\theta/\mathrm{Ca}^{1/3}$, for a range of values of Φ. We thus find a good agreement between the prediction of the corner model, without any adjustable parameters, and experiments. Note that strictly speaking the lubrication approximation is only valid in the limit of small slopes, while in the experiments one encounters angles up to 25°. One could thus expect minor quantitative differences.

The solid line in Fig. 5 has been obtained numerically, but it is possible to obtain an approximate description for the relation between θ and Φ, in the limit $\Phi\ll1$. Since at $\zeta=\tan\Phi$ one always encounters the boundary condition $H=0$, one can attempt a scaling solution of the form $H(\zeta)=c\hat{H}(\zeta/\tan\Phi)$; the argument of $\hat{H}$ can take values between -1 and 1. Since the radial fluid velocity, and hence H^2H'', should remain finite, we find that $c^3=\tan^2\Phi$. Inserting this scaling form in Eq. (10), one derives that at the symmetry axis $\hat{H}'''(0)\propto\tan^2\Phi$. The deviations from a simple parabola thus become increasingly small as $\Phi\to0$.[38] Combining a parabolic form of $H(\zeta)$ with the zero-flux condition $F(\zeta_c)=0$, [Eq. (11)], one obtains

$$\tan^3\theta = \frac{35}{16}\mathrm{Ca}\tan^2\Phi, \quad\text{when }\Phi\ll1, \tag{14}$$

which has been plotted as a dashed line in Fig. 5. Note that the prefactor of the parabolic approximation in Ref. 29 is slightly different, due to a planar approximation of the flow.
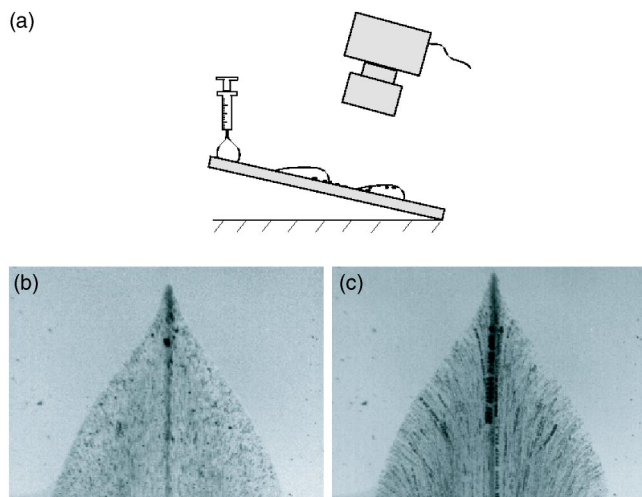
(a)

(b)   (c)

FIG. 6. (a) Schematic picture of the experiment; drops of silicon oil are deposited on an inclined plate covered with tracer particles. (b) The drops are filmed from above using a charge-coupled device (CCD) camera. (c) The trajectories of the tracers in the frame attached to the inclined plane obtained from superposition of successive images. Note that the trajectories start perpendicular to the contact line.

IV. PARTICLE IMAGE VELOCIMETRY MEASUREMENTS

In order to test the self-similar corner model in more detail we now present experimental measurements of the velocity profile at the rear of sliding drops, obtained by PIV. In Fig. 1 we have already seen that the experimental and theoretical flow fields are qualitatively very similar. In this section we provide a more quantitative comparison and indeed confirm the self-similarity of the velocity field in the experimentally accessible range.

A. Experimental setup

To visualize the velocity field at the rear of sliding drops, we performed experiments on partially wetting drops containing tracer particles. The experimental setup is sketched in Fig. 6. We consider millimeter-sized drops of silicon oil ($\eta = 50$ cP; $\gamma = 20$ mN m^{-1}), sliding down an inclined glass plate coated with fluoropolymers (FC725, sold by 3M). These conditions are the same as in Refs. 23 and 24, and provide a situation of partial wetting with a relatively small hysteresis of static contact angles (θ_{eq} between 45° and 52°). When sliding at a velocity $U_0 = 3$ mm/s (Ca = 0.0075), the drops exhibit a corner at the rear. Particles with diameters ranging from 1 to 10 μm are homogeneously dispersed on the plate, so that a passing drop drags the particles downwards. This way, the majority of the tracers remain either at the free surface of the drop or at the solid-liquid interface.

The trajectories of the tracers in the frame attached to the inclined plane can now be visualized by superimposing images obtained at different times. We can already note from Fig. 6(c) that these trajectories leave the contact line perpendicularly, as was anticipated in Sec. III. A quantative measurement of the local fluid velocity can now be obtained by particle image velocimetry, using the correlations between two successive pictures; the results presented in this paper were obtained by averaging over 20 pictures. Such measurements on drops exhibiting a corner are rather difficult since the presence of the tracers perturbs the shape of the drop near the corner tip and induces pearling, i.e., emission of little droplets. We have therefore been limited to a measurement on a drop that exhibits a cusp-like structure at the rear (Fig. 6). As will be shown below, this does not seem to perturb the velocity field in the region away from the cusp.

The fact that not all tracers are localized at the free surface makes it difficult to access the absolute values of the velocities. The velocity field in the vertical z direction is Poiseuille-like, which has a maximum at the free surface and is zero at the plate. One effectively averages over tracers at different heights, but the precise distribution of particles cannot be controlled. Although this leads to an uncertainty for the absolute values, the direction of the velocity at a given horizontal position (x, y) will be independent of the height. Therefore, the angle Ψ defining the orientation of **U** can be measured with a much greater precision and will be the central quantity of our study—the definition of Ψ is provided in Fig. 7(c). We furthermore obtain interesting results for the velocity components as well, albeit with more experimental noise.

B. Experimental results

The main prediction of the corner model is that the velocity field should be independent of the distance to the corner tip. To verify this self-similarity, we have plotted the experimental results with different symbols according to the distance to the tip; the slices drawn in Fig. 7(a) each have a width of 52 μm. Note that we have defined the origin $(x, y) = (0, 0)$ by extrapolating the straight contact lines away from the cusp. We first consider the orientation of the velocity field, Ψ, as a function of the position φ. The data shown in Fig. 7(c) indeed collapse onto a master curve that is independent of the distance from the corner tip. The velocity field in the corner regime is indeed self-similar, at least within the experimentally accessible range, which comprises at least half a decade (from 52 to 312 μm). As a further test of the corner model, we imposed the curve Ψ as a function of φ obtained from the model for $\Phi = 35°$ (solid line). Given the fact that there are no adjustable parameters, this curve is in very good agreement with the experimental data; small differences could be due to the assumption of small slopes underlying the lubrication approximation.

In Fig. 8 we have plotted the velocity components U_r and U_φ as a function of the position φ. These measurements are obtained from an average over particles at different heights, and therefore are much more scattered than the data for Ψ. To account for this averaging we have furthermore rescaled the data by an empirical factor of $1.15 U_0$; if all particles would be localized at the free surface, one would require a factor of $3 U_0 / 2$. Although the data are rather noisy, the results are consistent with the velocity fields obtained from the corner model (solid and dashed lines). In particular, it is clear that the radial velocity at the contact line vanishes, so that at the contact line the fluid velocity is truly perpendicular.
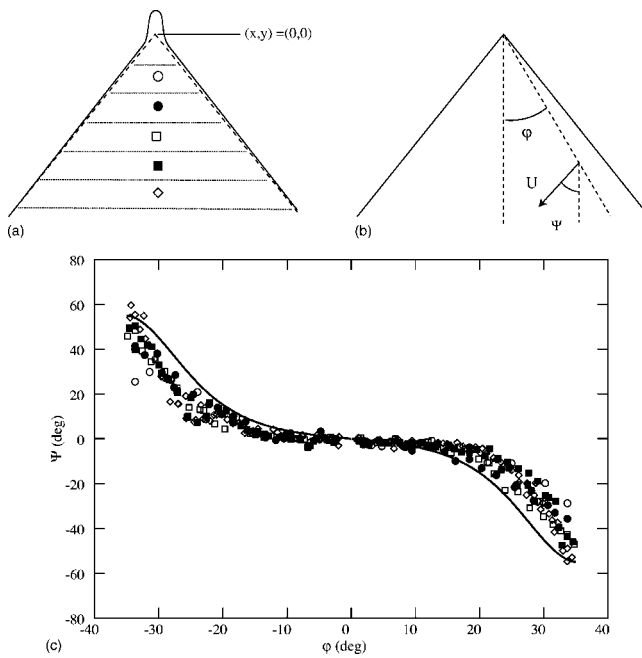
FIG. 7. (a) To test the self-similarity of the velocity, we have divided our data into slices of 52-μm width, at different distances from the corner tip. The position of the tip is defined by extrapolation of the contact lines away from the cusp. (b) Definition of Ψ, the orientation of the local fluid velocity **U**. (c) The experimental data for Ψ as a function of φ collapse on a single curve, due to the self-similarity of the velocity field. This master curve is in good agreement with the prediction of the corner model.

V. REAR OF THE DROP: A MODEL FOR CURVED CONTACT LINES

In Sec. IV B we have seen that the self-similar conical model provides a very good description of the flow within the corner. To be precise, it agrees with the experimental data in the regime where the contact lines on both sides of the symmetry axis are nearly straight. However, the contact line at the rear of the drop never forms an infinitely sharp corner, but was found to have a well-defined radius of curvature R (see Fig. 2). The experimental data of Ref. 35 have been
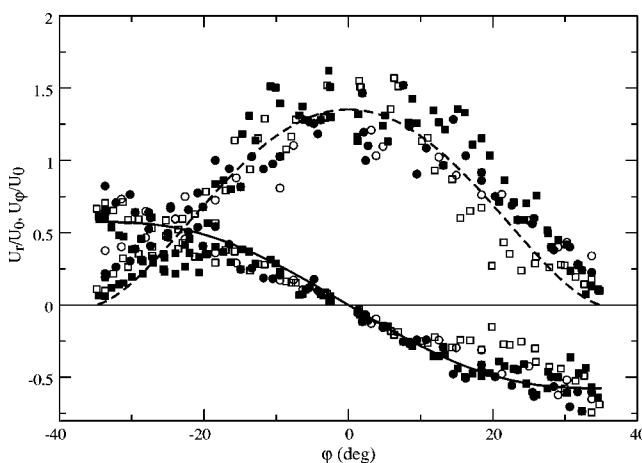

FIG. 8. Velocity components U_r and U_φ obtained experimentally at different distances from the corner tip (symbols), compared to the theoretical model (dashed and solid lines, respectively). The radial velocity vanishes at the contact line, indicating a locally perpendicular fluid velocity.

reproduced in Fig. 9; while the contact line curvature remains almost constant at low Ca, one observes a dramatic increase of $1/R$ when the singularity is formed at the rear. A similar curve is obtained for the contact angle θ, which has been measured at a macroscopic scale. It is well known that this macroscopic angle decreases for increasing Ca, and the experimental results in Fig. 10 clearly show that the transition to the corner occurs at a nonzero angle.

These observations provoke two fundamental questions. First, it is found experimentally that the corner angle adjusts itself such that the normal velocity, Ca sin Φ, remains at the maximum speed of dewetting Ca_c (Refs. 20 and 24) (see Fig. 2). The contact lines away from the rear are thus inclined with respect to the horizontal in order to avoid entrainment. At the rear, however, the local velocity of the contact line *does* exceed this maximum speed Ca_c, but still the drop does not leave a film or little drops. A first problem is thus to understand why curved contact lines can avoid entrainment, even above Ca_c. A second intriguing observation is that the length scale R at which the corner singularity is regularized (≈ 100 μm) is neither the capillary length nor the microscopic molecular length; what determines the length scale of R?

To address these questions we will develop a description of *curved moving contact lines*, in which the transverse curvature effects are taken into account up to the lowest order. We indeed find that the transition to entrainment is postponed by curving the contact line, and our results are consistent with experiments.

A. 1D lubrication equation for curved contact lines

Let us consider the effect of contact line curvature right *at the symmetry axis of the drop*. The governing lubrication equation becomes

$$\frac{\partial}{\partial x} \left(\partial_{xx} h + \partial_{yy} h \right)\big|_{y=0} = \frac{3\eta}{\gamma} \frac{U_x}{h^2}, \qquad (15)$$

which, in fact, is the x component of Eq. (6) at $y=0$. The x component of the velocity, U_x, is equal to the global speed U_0 at the rear of the drop, while in the self-similar corner regime it is slightly larger than U_0 (see Fig. 4). In order to keep the discussion transparent, however, we simply take $U_x=U_0$ to be constant throughout the analysis—in the Appendix we demonstrate that this hardly affects our results.

For a straight contact line one trivially has $\partial_{yy}h=0$, so that the problem becomes purely one dimensional, in the sense that there is only a dependence on x. For curved contact lines, however, this transverse curvature term gives a nonzero contribution and starts to play an important role when increasing $1/R$. In the Appendix we derive that $\partial_{yy}h = -h/(xR)$ up to the lowest order in $1/R$, so that one still has a closed one-dimensional description of the problem. This lowest-order contribution of the contact line curvature can be interpreted as a parabolic approximation of the cross section at a given distance from the rear x, but it is possible to show more rigorously that
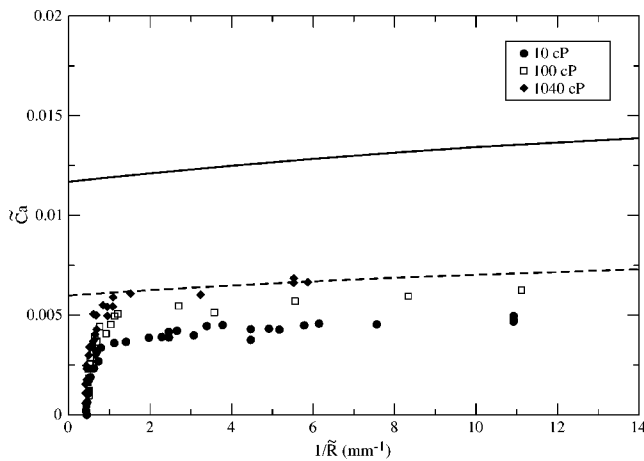
FIG. 9. The symbols are experimental data of contact line curvature $1/\tilde{R}$ vs $\tilde{C}a$ on drops of silicon oil.[35] ($\tilde{C}a=Ca/\tan^3 \theta_{eq}$; $\tilde{R}=R\tan\theta_{eq}$). The curvature suddenly increases dramatically when approaching a critical $\tilde{C}a_c$. The solid line represents the theoretical prediction for the maximum capillary number from Eq. (17); $\tilde{C}a_c$ can only increase by dramatically increasing $1/\tilde{R}$. The numerical values of $\tilde{C}a_c$ are not well predicted by the solid line, but a quantative agreement can be obtained by slightly modifying the microscopic boundary condition (dashed line, see text).

$$\partial_{xyy} h|_{y=0} = \frac{1}{xR}\left(\frac{h}{x} - \partial_x h\right) + \mathcal{O}\left(\frac{1}{R^2}\right). \qquad (16)$$

The higher-order terms originate from deviations from the parabolic shape, and can only be computed from a complete analysis incorporating the y dependence.

After rescaling the x direction with respect to the equilibrium contact angle, $\tilde{x}=x\tan\theta_{eq}$, we thus find the following one-dimensional equation for curved contact lines:

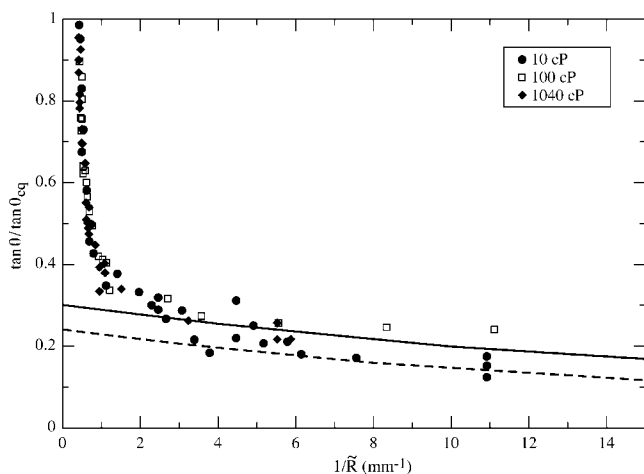FIG. 10. The symbols are experimental data of contact line curvature $1/\tilde{R}$ vs macroscopic contact angle θ (Ref. 36). The solid line represents the minimum contact angle from Eq. (17); the contact angle can only continue to decrease by dramatically increasing $1/\tilde{R}$. The dashed line was obtained with a slightly modified microscopic boundary condition (see text).

$$h''' + \frac{1}{\tilde{R}\tilde{x}}\left(\frac{h}{\tilde{x}} - h'\right) = \frac{3\tilde{C}a}{h^2}, \qquad (17)$$

where $\tilde{C}a=Ca/\tan^3 \theta_{eq}$ and $\tilde{R}=R\tan\theta_{eq}$. Since h and $\tilde{x}$ are of the same order, it is clear that the curvature term will start to play a role when $\tilde{R}$ and h become of the same order of magnitude. At small heights, i.e., $h\ll\tilde{R}$, the curvature term will thus be small compared to the viscous term and the physics reduces to that of a straight contact line. For experimental measurements performed at a macroscopic scale $h=L$, the relevant dimensionless parameter will thus be $L/\tilde{R}$.

Before we continue the analysis, let us try to understand qualitatively how the extra curvature term affects the hydrodynamics of curved contact lines. For receding contact lines, the slope of the interface decreases when increasing the height of the drop, i.e., $\theta_{macro}<\theta_{micro}$. Therefore, the local slope h' will always be smaller than $h/\tilde{x}$ so that the $1/\tilde{R}$ term in Eq. (17) gives a positive contribution to the capillary forces. In the opposite case of $\theta_{macro}>\theta_{micro}$ this contribution becomes negative. We thus anticipate that contact line curvature provides an additional capillary driving mechanism in the case of receding contact lines, which helps to postpone the forced wetting transition. For advancing contact lines, on the other hand, it behaves as an additional source of dissipation.

B. Boundary conditions

A hydrodynamic description of moving contact lines raises the fundamental difficulty of the singularity as $h\rightarrow 0$, due to the divergence of the viscous forces. This singularity should be resolved on a microscopic, molecular length scale l, for example, by introducing slip boundary conditions.[15,16] In the spirit of Voinov we assume that, apart from viscosity, there are no additional microscopic dissipation mechanisms, so one can impose the equilibrium contact angle θ_{eq} at this microscopic scale l.[3] It was furthermore shown by Eggers that the macroscopic physics is only weakly dependent on the precise slip law, so we are allowed to boldly cut the solutions at $h=l$.[16,39] In rescaled coordinates we thus encounter $h'=1$ at $h=l$ at $x_0\approx l$ ($x=0$ corresponds to the position of the contact line). At the end of this section we come back to the validity of these two boundary conditions. Depending on the chemical composition of the fluid, this microscopic length should range from nanometers to several tens of nanometers, and we therefore take $l=10^{-8}$ m.[23,24]

To close the problem we should provide a third boundary condition, which in general depends on the global properties of the droplet. Our description up to the lowest order in the curvature is only valid in the vicinity of the contact line, and hence, we cannot rigorously match the solutions of Eq. (17) to the global behavior of the drop. However, it was recently demonstrated that the critical capillary number for the problem of a plate withdrawn from a bath only weakly depends on the global geometry;[16] the explicit dependence on the inclination angle of the plate shows up as a logarithmic factor. This allows us to perform the following semi-quantitative analysis. The solutions of Eq. (17) should cross-

over to the corner solutions, which have $\partial_{xx}h=0$ at a macroscopic scale L. In order for the solutions to have sufficient overlap, we therefore take $h''=0$ at $h=L$ as the third boundary condition for Eq. (17). Such an *ad hoc* boundary condition indeed provides a reasonable estimate for $\widetilde{Ca}_c$; for straight contact lines we numerically obtain that $\widetilde{Ca}_c$ scales roughly as $1/\ln(L/l)$, and the precise values lie within 30% (Ref. 40) of the exact results of Ref. 16. Although our approach is not rigorous, we are confident that it provides a semi-quantitative description of the dynamics of curved contact lines.

Since in typical experiments the maximum height of the drops is less than a millimeter, we take $L=10^{-4}$ m, so that $L/l=10^4$. However, let us make the following important remark. *A priori*, it is not clear at what scale the curved contact line solutions should be matched to the self-similar corner solutions. This matching should occur well below the capillary length (≈ 1 mm), but in principle it could be much smaller than the experimental scale L. If this were the case, however, one should even find smaller values of R than those presented in our paper. In this respect, our analysis possibly underestimates the curvature of the contact line at the rear. We come back to this point in the Discussion at the end of the paper.

C. The entrainment threshold for finite R

To investigate how the extra curvature term affects the dynamics of receding contact lines, we have numerically evaluated Eq. (17) for different values of $1/\widetilde{R}$, with the parameters specified in the preceding paragraph. We found that beyond a certain value of the capillary number $\widetilde{Ca}_c$, there no longer exist solutions consistent with the imposed boundary conditions. This corresponds to the maximum speed of dewetting or the entrainment threshold.[14–16] Interestingly, this $\widetilde{Ca}_c$ depends on the curvature of the contact line; the solid line in Fig. 9 shows that $\widetilde{Ca}_c$ increases with $1/\widetilde{R}$. This implies that the drop can avoid entrainment by increasing the contact line curvature at the rear.

This entrainment threshold occurs at a nonzero macroscopic slope,[14] i.e., $h'\neq 0$ at $h=L$. In Fig. 10 we plot this critical slope, $\tan\theta_c$, as a function of $1/\widetilde{R}$ (solid line); the critical contact angle decreases as a function of the contact line curvature. This is in good agreement with the symbols representing experimental measurements of the macroscopic contact angle as a function of $1/\widetilde{R}$. This angle is first observed to decrease continuously, due to an increase of $\widetilde{Ca}$, without significant changes of the contact line curvature. Approaching the critical speed of dewetting, however, a further decrease of the contact angle has to be accompanied by a dramatic increase of the contact line curvatures. This increase is well predicted by Eq. (17). The experimental data do not extend below $R\approx 80$ μm, around which a cusp is formed at the rear of the drop and small droplets are emitted.

Analyzing the experimental data in terms of the capillary number, however, we find a striking quantitative discrepancy with the prediction of our model; the experimental data shown in Fig. 9 follow a similar trend as the theoretical

curve (solid line) but the numerical values of $\widetilde{Ca}_c$ differ by about a factor of 2.[41] Let us now make the following observation. Within the lubrication theory, the numerical value of the critical capillary number is very sensitive to the microscopic boundary condition on $\partial_x h|_l$, since $Ca_c=\widetilde{Ca}_c(\partial_x h|_l)^3$. That is, if the slope of the interface at a microscopic scale would be about 20% smaller than the equilibrium contact angle θ_{eq}, one would already lower the critical capillary number by a factor of 2. This is illustrated by the dashed curve in Fig. 9, which has been obtained from the microscopic boundary condition $h'=0.8$ (instead of $h'=1$). Given the fact that overall, the theoretical predictions of the lubrication theory work very well, the experimental data suggest that at high Ca, the microscopic contact angle starts to deviate significantly from θ_{eq}.

D. Qualitative features from energy balance

As was shown by de Gennes,[14] one can obtain a simplified, but very insightful description of dynamic contact lines from a global energy balance. Formally one would obtain a depth-averaged energy balance by multiplying both sides of Eq. (17) by hU_0, and integrating once from a microscopic to a macroscopic position x. By estimating the contribution of each of the terms, one already captures qualitative features of the physics. Note that different approaches or approximations can lead to slightly different laws for the macroscopic contact angle as a function of Ca.[3,4,6] Our aim here is not to fine-tune any of these models, but just to illustrate how contact line curvature might affect the dynamics.

One can estimate the integrated viscous dissipation by approximating the geometry near the contact line by a wedge with a macroscopic contact angle θ; this yields $3\eta U_0^2\ln(L/l)/\tan\theta$. Without the $1/\widetilde{R}$ term, this dissipation should be compensated by the unbalanced Young force $\gamma U_0(\cos\theta-\cos\theta_{eq})$, resulting into de Gennes' law for the macroscopic or dynamic contact angle θ.[14] Even though this argument ignores the strong curvatures of the interface it does capture the entrainment transition at a nonzero contact angle, as observed for the sliding drops (Fig. 10). Note, however, that the predicted angle, $\theta_c=\theta_{eq}/\sqrt{3}$, is somewhat larger than those observed experimentally.

Let us now estimate the contribution of the additional term in Eq. (17). In Sec. V A we argued that this term provides additional capillary forces for receding contact lines ($\theta<\theta_{eq}$), while it favors dissipation for advancing contact lines ($\theta>\theta_{eq}$). At low speeds we can therefore expect the integrated contribution to scale as $(\theta_{eq}-\theta)/R$, so that we obtain a modified energy balance,

$$\left(\theta_{eq}^2-\theta^2+\alpha\frac{L}{R}[\theta_{eq}-\theta]\right)=\frac{6Ca\ln(L/l)}{\theta}, \tag{18}$$

where we have developed $\cos\theta$ for small θ. The factor L emerges from the integration from l to L, and α is expected to be of order unity.

Although the linear correction term in Eq. (18) can only be justified in the limit of small Ca, it is interesting to see that Eq. (18) indeed predicts a shift of the entrainment
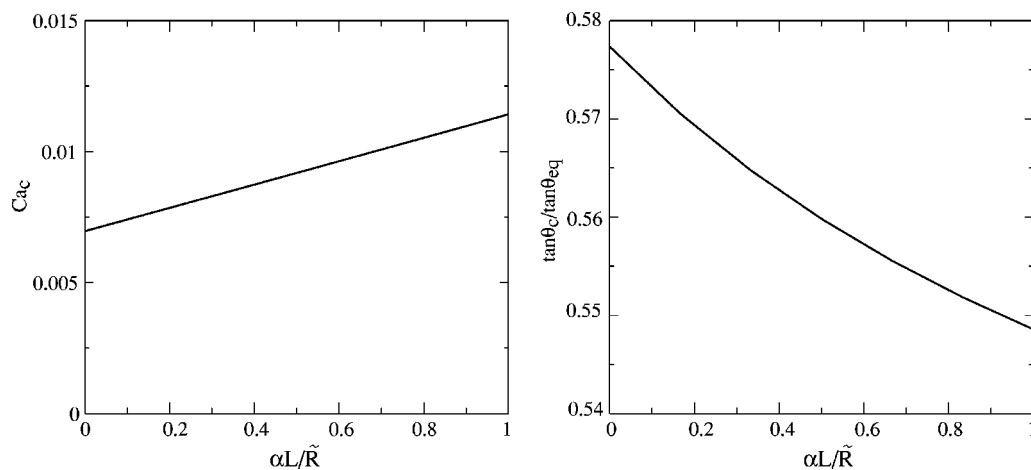
FIG. 11. The critical capillary number, $\widetilde{Ca_c}$, and critical slope, $\tan\theta_c/\tan\theta_{eq}$, as a function of the dimensionless contact line curvature $\alpha L/\tilde{R}$ obtained from Eq. (18). These features are in qualitative agreement with full simulations of Eq. (17).

threshold due to curvature of the contact line. This is illustrated in Fig. 11 where we plot Ca_c and the miminum angle θ_c as a function of the curvature, computed from Eq. (18). This qualitatively reproduces the features of the full numerical integration in Figs. 9 and 10.

VI. DISCUSSION

In this paper we have analyzed the three-dimensional flow and morphology of the corner singularity at the rear of sliding drops. We have provided a detailed comparison between theoretical predictions from similarity solutions of the lubrication equations, and direct experimental measurements. The relevance of the similarity solutions is emphasized by the excellent agreement for the nontrivial velocity field at the rear of the drop. A striking feature of this flow is that the fluid velocity at the contact line is always oriented perpendicularly to the contact line, while its absolute value coincides with the normal velocity of the contact line.

We furthermore analyzed the transition from rounded to cornered drops, by developing a model for curved contact lines. We found that the forced wetting transition can be postponed by increasing the curvature of the contact line at the rear of the drop. This strongly curved part serves as a small-scale regularization of the corner singularity, and its typical length scale R decreases rapidly when Ca approaches the transition. The general scenario is thus that *the drop can avoid the forced wetting transition* by simultaneously developing a strongly curved contact line at the rear of the drop, and the straight inclined contact lines at the sides. This morphology mobilizes additional capillary driving forces due to interface curvatures perpendicular to the direction of the flow.

The results presented in this paper strongly suggest that the structure and the flow in the corner are entirely governed by a balance between viscous and capillary forces. This contrasts the approach by Ben Amar, Cummings, and Pomeau,[34] in which all viscous forces are assumed to be effectively localized at the contact line so that the shape of the free surface follows from a balance between gravity and surface tension. While this assumption allows us to resolve the glo-

bal shape of the drop, it cannot be expected to describe structures of scales below the capillary length. For example, the existence of a purely conical shape [Fig. 2(c)] crucially requires viscosity; a balance between gravity and surface tension would yield a strongly convex side view.[34] To further quantify this we have estimated the distance from the contact line at which gravity and viscous forces attain the same magnitude, directly from our experimental data.[42] Figure 12 clearly shows that viscosity dominates over gravity in basically the entire corner region.

Let us also mention that there exist fully two-dimensional numerical simulations using a disjoining pressure with a precursor film, in which cusping droplets have been observed.[22,43] At present, however, such simulations can only incorporate a limited spatial resolution, i.e., $l_{micro}/l_\gamma \sim 10^{-2}$, and appear to miss the experimentally observed evolution of the corner singularity as a function of Ca. In this paper we avoid this numerical problem by residing to one-dimensional descriptions of the two-dimensional flow, which allows resolving the physically relevant length scales.

The present work provokes a number of questions. The critical values of Ca predicted by the curved contact line model differ by about a factor of 2 from the experimental values. A similar disagreement was encountered by Hocking for the problem of a plate withdrawn from a bath.[15] We suggest that this may provide fundamental information on the microscopic boundary conditions; one recovers the experimental results when taking a microscopic contact angle slightly below the equilibrium angle θ_{eq}. It would be interesting to see whether this could be captured by including a microscopic disjoining potential.[7,8,21,22,44] Such an approach allows us to explicitly incorporate microscopic physics, from which effective microscopic boundary conditions emerge without additional assumptions. Results by Thiele, Velarde, Neuffer, Bestehorn, and Pomeau[21] and Thiele, Neuffer, Bestehorn, Pomeau, and Velarde[22] in which contact angles are observed to decrease with velocity even at very small scales, appear to be consistent with our findings. Another reason for the discrepancy may be that surface roughness, which has not been taken into account here, can lower the critical
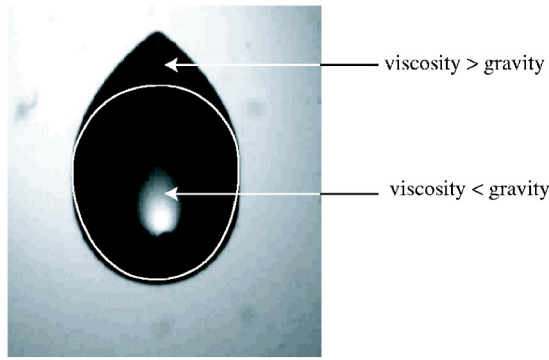
FIG. 12. One can separate the viscosity-dominated regime from the gravity-dominated regime by equating the corresponding terms in the full lubrication equation (Ref. 42). It is clear that viscous effects are dominant in the entire corner regime, and not only close to the contact line. The remarkable asymmetry between the front and the back of the drop has two origins: (i) $\partial h / \partial x > 0$ at the rear and therefore reduces the effect of gravity, while at the front $\partial h / \partial x < 0$, so that gravity is enhanced (Ref. 42). (ii) the macroscopic contact angles at the rear are much smaller than those at the front, resulting into larger distances to attain the cross-over height.

speed.[19] However, the values of the critical contact angle predicted by this theory are much larger than those observed experimentally.

Finally, we have not addressed the selection of the corner angle Φ as a function of the capillary number, which requires a proper matching of the singular behavior near the contact line to the global corner geometry. The difficulty is that a truly self-similar interface has no intrinsic length scale, and is incompatible with the usual wetting boundary conditions imposed at a microscopic scale. We speculate that the finite curvature at the rear effectively provides a length scale; only when R becomes orders of magnitudes smaller than the capillary length l_γ, which forms the macroscopic cutoff, the corner can no longer obey physical wetting boundary conditions. This would explain why the formation of a cusp emitting little drops coincides with $R/l_\gamma \rightarrow 0$.[35]

ACKNOWLEDGMENTS

APPENDIX: CURVED CONTACT LINES

In this appendix we derive the lowest-order term of the transverse capillary pressure $\partial_{yy} h$ for a moving contact line that has a finite radius of curvature R. We then show that gradients of the velocity $U_x(x)$ complicates the analysis presented in Sec. V, but that it has little impact on the results.

Since locally, the contact line can be described by a parabola $x = y^2/(2R)$, the relevant dimensionless variable in this problem will be $\xi = y/\sqrt{2Rx}$, which can range from -1 to 1. Without loss of generality, we parametrize the interface as

$$h(x,y) = f(x)[1 - \xi^2]\left[1 + \sum_{n=1}^{\infty} a_{2n}(x)\xi^{2n}\right]. \quad (A1)$$

The function $f(x)$ is simply the height profile at the symmetry axis of the drop, i.e., $h(x, y=0)$, while we write the cross section of the interface in a polynomial expansion. We have conveniently factored out the term that vanishes at the contact line. Note that the functions $f(x)$ and $a(x)$ implicitly depend on R; eventually, the goal is to determine how the center profile $f(x)$ is affected by a finite R.

In Eq. (15) we have to evaluate $\partial_{xyy} h$ at the symmetry axis $y=0$. Using the parametrization introduced above this becomes

$$\partial_{xyy} h|_{y=0} = -\frac{1}{R}\left[(1 - a_2)\partial_x\left(\frac{f}{x}\right) - a_2'\frac{f}{x}\right], \quad (A2)$$

and thus requires explicit knowledge of $a_2(x)$. Let us now make the following crucial observation. In order to avoid a singularity of the slope of the interface when going around the drop, it turns out that all $a(x)$ should vanish as $x \rightarrow 0$. For example, the contact angle θ at the rear of the drop simply follows from $\tan \theta = f'$, while elsewhere on the contact line

$$\tan \theta = |\nabla h|_{\xi=\pm1} = \frac{f(x)}{x}\left[1 + \sum_{n=1}^{\infty} a_{2n}(x)\right]\sqrt{1 + \frac{2x}{R}}. \quad (A3)$$

In order that θ varies continuously along the contact line, we thus require that $\Sigma a_{2n}(x)$ vanishes in the limit $x \rightarrow 0$. Repeating the same argument for contours at arbitrary fixed values $|\xi| < 1$, one finds that, in fact, all $a_{2n}(x)$ vanish individually at $x=0$.

We can thus write $a_2(x) \simeq a_2'x$, which should be of order $\mathcal{O}(x/R)$ since R provides the only length scale for a_n'. This results in the expression of Eq. (16),

$$\partial_x \partial_{yy} h|_{y=0} = \frac{1}{xR}\left(\frac{f}{x} - f'\right) + \mathcal{O}\left(\frac{1}{R^2}\right). \quad (A4)$$

Let us now address the approximation that $U_x(x) = U_0$ that was made in Sec. V. From the continuity equation it is clear that this approximation disregards the velocity component U_y: although U_y vanishes at the symmetry axis, the gradient $\partial_y U_y$ can be nonzero. To properly take these gradients into account one should thus incorporate continuity and start from Eq. (8). Using the parametrization of Eq. (A1) and keeping only the lowest order in $1/R$, we then obtain a fourth-order equation,

$$\partial_x[f^3 f'''] = 3\mathrm{Ca}f' + \frac{1}{R}\partial_x\left\{f^3\partial_x\left[\frac{f}{x}\right]\right\} + \frac{1}{R}f^3\partial_{xx}\left[\frac{f}{x}\right]. \quad (A5)$$

Without the last term on the right-hand side, one could immediately integrate this equation to Eq. (17). To investigate the effect of the extra term, we have numerically integrated this fourth-order equation; this yields results that are very similar to those presented in Sec. V. We have therefore preferred to discuss the physics of rounded drops using the simplified third-order equation instead of Eq. (A5).

[1]C. Huh and L. E. Shriven, "Hydrodynamic model of steady movement of a solid/liquid/fluid contact line," J. Colloid Interface Sci. **35**, 85 (1971).

[2]E. B. Dussan, V. Davis, and S. H. Davis, "On the motion of a fluid-fluid interface along a solid surface," J. Fluid Mech. **65**, 71 (1974).

[3]O. V. Voinov, "Hydrodynamics of wetting," Fluid Dyn. **11**, 714 (1976).

[4]R. G. Cox, "The dynamics of the spreading of liquids on a solid surface," J. Fluid Mech. **168**, 169 (1986).

[5]L. M. Hocking, "The spreading of a thin drop by gravity and capillarity," Q. J. Mech. Appl. Math. **36**, 55 (1983).

[6]T. D. Blake, J. De Coninck, and U. D'Ortuna, "Models of wetting: Immiscible lattice Boltzmann automata versus molecular kinetic theory," Langmuir **11**, 4588 (1995).

[7]L. M. Pismen and Y. Pomeau, "Disjoining potential and spreading of thin liquid layers in the diffuse-interface model coupled to hydrodynamics," Phys. Rev. E **62**, 2480 (2000).

[8]L. W. Schwartz, R. V. Roy, R. R. Eley, and S. Petrash, "Dewetting patterns in a drying liquid film," J. Colloid Interface Sci. **234**, 363 (2001).

[9]U. Thiele, K. John, and M. Bär, "Dynamical model for chemically driven running droplets," Phys. Rev. Lett. **93**, 027802 (2004).

[10]P. Seppecher, "A numerical study of a moving contact line in Cahn–Hilliard theory," Int. J. Eng. Sci. **34**, 977 (1996).

[11]Y. D. Shikhmurzaev, "Moving contact lines in liquid/liquid/solid systems," J. Fluid Mech. **334**, 211 (1997).

[12]Y. Pomeau, "Recent progress in the moving contact line problem: A review," C. R. Mec. **330**, 207 (2002).

[13]S. F. Kistler and P. Schweizer, *Liquid Film Coating—Scientific Principles and Their Technological Implications* (Kluwer, Dordrecht, 1997).

[14]P. G. de Gennes, "Deposition of Langmuir–Blodget layers," Colloid Polym. Sci. **264**, 463 (1986).

[15]L. M. Hocking, "Meniscus draw-up and draining," Eur. J. Appl. Math. **12**, 195 (2001).

[16]J. Eggers, "Hydrodynamic theory of forced dewetting," Phys. Rev. Lett. **93**, 094502 (2004).

[17]D. Quéré, "On the minimal velocity of forced spreading in partial wetting," C. R. Acad. Sci., Ser. II: Mec., Phys., Chim., Sci. Terre Univers, **313**, 313 (1991).

[18]L. D. Landau and B. V. Levich, "Dragging of a liquid by a moving plate," Acta Physicochim. URSS **20**, 17, 42 (1942); B. V. Derjaguin, "On the thickness of the liquid film adhering to the walls of a vessel after emptying," *ibid.* **20**, 349 (1943).

[19]R. Golestanian and E. Raphael, "Relaxation of a moving contact line and the Landau–Levich effect," Europhys. Lett. **55**, 228 (2001).

[20]T. D. Blake and K. J. Ruschak, "A maximum speed of wetting," Nature (London) **282**, 489 (1979).

[21]U. Thiele, M. G. Velarde, K. Neuffer, M. Bestehorn, and Y. Pomeau, "Sliding drops in the diffuse interface model coupled to hydrodynamics," Phys. Rev. E **64**, 061601 (2001).

[22]U. Thiele, K. Neuffer, M. Bestehorn, Y. Pomeau, and M. G. Velarde, "Sliding drops on an inclined plane," Colloids Surf., A **206**, 87 (2002).

[23]T. Podgorski, J. M. Flesselles, and L. Limat, "Corners, cusps and pearls in running drops," Phys. Rev. Lett. **87**, 036102 (2001).

[24]A. Daerr, N. Le Grand, L. Limat, and H. A. Stone, "Drops sliding along an inclined plane: Experiments versus 3D hydrodynamical model," Proceedings of the Fifth European Coating Symposium, 17–19 September 2003, Polytype Converting, Friburg, 2004, edited by P. M. Schweizer.

[25]U. Thiele and E. Knobloch, "Front and back instability of a liquid film on a slightly inclined plate," Phys. Fluids **15**, 892 (2003).

[26]A. G. Gonzales, J. Diez, J. Gomba, R. Gratton, and L. Kondic, "Spreading of a thin two-dimensional strip of fluid on a vertical plane: Experiments and modeling," Phys. Rev. E **70**, 026309 (2004).

[27]G. Reiter and A. Sharma, "Auto-optimization of dewetting rates by rim instabilities in slipping polymer films," Phys. Rev. Lett. **87**, 166103 (2001).

[28]H. A. Stone, L. Limat, S. K. Wilson, J.-M. Flesselles, and T. Podgorski, "Corner singularity of a contact line moving on a solid surface," C. R. Phys. **3**, 103 (2002).

[29]L. Limat and H. A. Stone, "Three-dimensional lubrication model of a contact line corner singularity," Europhys. Lett. **65**, 365 (2004).

[30]X. D. Shi, M. P. Brenner, and S. R. Nagel, "A cascade structure in a drop falling from a faucet," Science **265**, 157 (1994); M. Brenner, J. R. Lister and H. A. Stone, "Pinching threads, singularities and the number 0.0304...," Phys. Fluids **8**, 2827 (1996); J. Eggers, "Nonlinear dynamics and breakup of free-surface flows," Rev. Mod. Phys. **69**, 865 (1997).

[31]I. Cohen and S. R. Nagel, "Scaling at a selective withdrawal transition through a tube suspended above the fluid surface," Phys. Rev. Lett. **88**, 074501 (2002); W.W. Zhang, "Viscous entrainment from a nozzle: Singular liquid spouts," *ibid.* **93**, 184502 (2004).

[32]J. Eggers, "Air entrainment through free-surface cusps," Phys. Rev. Lett. **86**, 4290 (2001); E. Lorenceau, F. Restagno, and D. Quéré, "Fracture of a viscous liquid," *ibid.* **90**, 184501 (2003).

[33]E. Rio, A. Daerr, B. Andreotti, and L. Limat, "Boundary condition in the vicinity of a dynamic contact line," Phys. Rev. Lett. **94**, 024503 (2005).

[34]M. Ben Amar, L. J. Cummings, and Y. Pomeau, "Transition of a moving contact line from smooth to angular," Phys. Fluids **15**, 2949 (2003).

[35]Recent experiments show that as the corner develops, there is a tremendous increase of contact line curvature in a very narrow range of Ca. These results will be published in a forthcoming paper, by the same authors as of Ref. 24.

[36]Note that the curve $H(\zeta)$ vs $F(\zeta)$ is different from the one presented in Ref. 29, which had a problem with numerical precision. However, the conclusions remain unaltered.

[37]In the frame comoving with the droplet, mass conservation requires that the total flux across a cross section vanishes, cf. Eq. (11). Since at the contact line the downward velocity U_x is smaller than the global drop speed U_0, this locally corresponds to an "upstream" velocity in the comoving frame. To compensate for this, the velocity at $\varphi = 0$ will be larger than U_0.

[38]The solutions never become purely parabolic; Eq. (12) shows that the higher-order derivatives become dominant close to the contact line. However, our numerical curves indicate that deviations from a simple parabola become increasingly localized to the contact line when $\Phi \rightarrow 0$.

[39]J. Eggers, "Toward a description of contact line motion at higher capillary numbers," Phys. Fluids **16**, 3491 (2004).

[40]We have compared our results for $\tilde{C}a_c$ to Eq. (9) of Ref. 16, by taking $L = l_\gamma/10$ (l_γ being the capillary length) and by varying the geometric parameter $\theta_{eq}^2/\theta_{plate}$ from 0.1 to 10.

[41]Note that for increasing viscosity, which in this case corresponds to an increasing microscopic length l of the silicon oil polymer chains, the critical capillary number is slightly increasing. This is consistent with the typical scaling of $Ca \propto 1/\ln(L/l)$.

[42]We have equated the absolute values of the viscous term, $3\eta U/(\gamma h^2)$, and the gravitational term, $(\sin \alpha \mathbf{e}_x - \cos \alpha \nabla h)/l_\gamma^2$, which appear in the full lubrication equation. This provides an objective cross-over height that is determined directly from experimental measurements; close to the contact line we know the slope ∇h from measurements using a laser sheet,[33] α is the inclination angle of the plane, while $|\mathbf{U}|$ is simply the normal velocity of the contact line.

[43]M. Bestehorn and K. Neuffer, "Surface patterns of laterally extended thin liquid films in three dimensions," Phys. Rev. Lett. **87**, 046101 (2001).

[44]P. G. de Gennes, X. Hua, and P. Levinson, "Dynamics of wetting: Local contact angles," J. Fluid Mech. **212**, 55 (1990).